ACS AuthorChoice

Novel Functionalization of Discrete Polymeric Biomaterial Microstructures for Applications in Imaging and Three-Dimensional Manipulation

James R. Pinney,[†,⊥] Gerd Melkus,[‡,§] Alec Cerchiari,[†,⊥] James Hawkins,[‡] and Tejal A. Desai*[,†]

[†]Bioengineering and Therapeutic Sciences, University of California, San Francisco, 1700 Fourth Street, Byers Hall Room 203, San Francisco, California 94158, United States

[‡]Department of Radiology, UCSF Imaging Center at China Basin, University of California, San Francisco, 185 Berry Street, Suite 190, Lobby 6, San Francisco, California 94107, United States

[§]Department of Medical Imaging, Ottawa Hospital, 1053 Carling Avenue, Ottawa K1Y 4E9, Ontario, Canada

[⊥]UC Berkeley-UCSF Graduate Program in Bioengineering, 1700 Fourth Street, Byers Hall Room 216, San Francisco, California 94158, United States

🅢 *Supporting Information*

ABSTRACT: Adapting ways to functionalize polymer materials is becoming increasingly important to their implementation in translational biomedical sciences. By tuning the mechanical, chemical, and biological qualities of these materials, their applications can be broadened, opening the door for more advanced integration into modern medical techniques. Here, we report on a method to integrate chemical functionalizations into discrete, microscale polymer structures, which are used for tissue engineering applications, for in vivo localization, and three-dimensional manipulation. Iron oxide nanoparticles were incorporated into the polymer matrix using common photolithographic techniques to create stably functional microstructures with magnetic potential. Using magnetic resonance imaging (MRI), we can promote visualization of microstructures contained in small collections, as well as facilitate the manipulation and alignment of microtopographical cues in a realistic tissue environment. Using similar polymer functionalization techniques, fluorine-containing compounds were also embedded in the polymer matrix of photolithographically fabricated microstructures. The incorporation of fluorine-containing compounds enabled highly sensitive and specific detection of microstructures in physiologic settings using fluorine MRI techniques (^{19}F MRI). These functionalization strategies will facilitate more reliable noninvasive tracking and characterization of microstructured polymer implants as well as have implications for remote microstructural scaffolding alignment for three-dimensional tissue engineering applications.

KEYWORDS: tissue engineering, 3D alignment, SPION, ^{19}F MRI, biomaterial, microrods, polymer functionalization
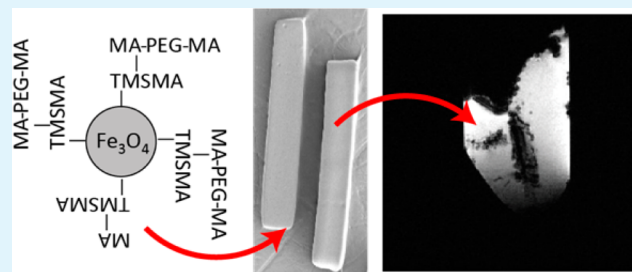
INTRODUCTION

Biocompatible polymeric materials have long been studied as a platform to improve the body's immune-tolerance and benign integration of implantable biomedical devices. Many of these materials also possess tunable mechanical properties and a minimally immunogenic profile, enabling them to find uses as nonreactive surface coatings,[1−4] drug delivery vehicles,[5−7] and structural components of implantable systems.[8−10] More recently, there has been increased interest in developing polymer biomaterials for applications in tissue engineering as in vitro and in situ cell scaffolds and as local modulators of cell responses and tissue characteristics.[11−15] Artificial long-chain biopolymers are often used for these purposes as they can possess these desirable characteristics, but they have also had limited therapeutic applications in part due to the inability to

dynamically and noninvasively manipulate them once embedded in the tissue.

One common construct that applies artificial long-chain biopolymers are hydrogel networks. These constructs can be porous in nature and therefore enable physiologically relevant cell growth in a 3D environment.[10,14] This approach has been adapted for numerous proposed therapies, notably in the setting of supportive cardiac strategies for the treatment of myocardial infarction, such as the delivery of bulk hydrogels for mechanical support of the injured myocardium[16−20] or implantation of discrete polymeric microstructures for alteration of the fibrotic cascade at the cellular level.[21−23] However,

the randomized nature of bulk polymer delivery and the uncontrolled orientation of discrete microstructural cues make these systems unpredictable directors of cell migration and tissue growth. This can lead to disorganized colonization of the polymer scaffold, which could precipitate pathogenic electrical developments in the regenerated tissue.[24] The ability to dynamically control injectable polymer therapies remotely could provide a means to address this shortcoming, facilitating the directed and organized growth of cells along tissue planes in a three-dimensional setting.

An additional obstacle to translational applications of implantable polymers is the difficulty in ensuring appropriate delivery localization and, in many cases, degradation rates of the implanted material. Tissue engineered scaffolds and devices are often engineered to be delivered by minimally invasive mechanisms such as polymerization or spreading upon injection into the target site.[16–20,25] Common hydrogel polymers, such as polyethylene glycol dimethacrylate (PEG–DMA), often have a density and hydration content[26] that is similar to that of the surrounding native tissue after they are delivered, making them nearly invisible to commonly used imaging modalities. Thus, there exists a need to functionally alter the chemical makeup of these materials to enable their localization after implantation without affecting the physical material characteristics that are vital to tissue engineering applications.

In this work, we utilized established polymer chemistry techniques to design functional biomaterials for tissue engineering and imaging applications. Through the incorporation of both iron oxide nanoparticles and fluorine-containing compounds, we sought to demonstrate unique capabilities of remote manipulation and MRI localization. This was achieved through the use of physiologically relevant MRI studies to establish the imaging proof of principle as well as the influence of permanent magnetic fields to facilitate coordinated movement of PEG–DMA microstructures. These chemical modifications could be adapted to a variety of biocompatible polymers used in medical technology, offering broad applications across a wide range of biomedical devices for implantation. In turn, this may reveal expanded opportunities for the implementation of functional biomaterials to create minimally invasive, tissue-engineered implantable therapeutics.

EXPERIMENTAL DETAILS

Silane–PEGDMA Polymer Synthesis. To produce polymer-coated iron oxide nanoparticles that facilitate chemical integration and miscibility in the PEG–DMA precursor solution for photolithographically fabricated microrods, a technique for silane–PEG diblock copolymer synthesis was adapted from Lee et al.[27] In brief, PEG–DMA (M_N = 750, Sigma) was mixed in an equimolar concentration with 3-(trimethoxysilylpropyl methacrylate) (Sigma) in tetrahydrofuran (THF, Sigma) in a pure nitrogen atmosphere. Following this, 2,2′-azobis(isobutyronitrile) (AIBN, Sigma) was added, and the mixture was placed on a hot plate at 70 °C for 24 h to induce free radical polymerization of the methacrylate groups and evaporate the THF solvent. This solution, poly(TMSMA-r-PEGDMA), was stored at 4 °C and is shown schematically in Figure 1A.

Polymer-Coated Iron Oxide Nanoparticle Synthesis. Iron oxide nanoparticles were synthesized through a base-initiated coprecipitation of two iron salts, as adapted from Lee et al.[28] with relative iron concentrations to dictate nanoparticle size guided by the work of Zhu et al.,[29] resulting in polymer-coated iron oxide nanoparticles, as represented in Figure 1A, and stored at 4 °C until further use (see Supporting Information). Iron content was measured
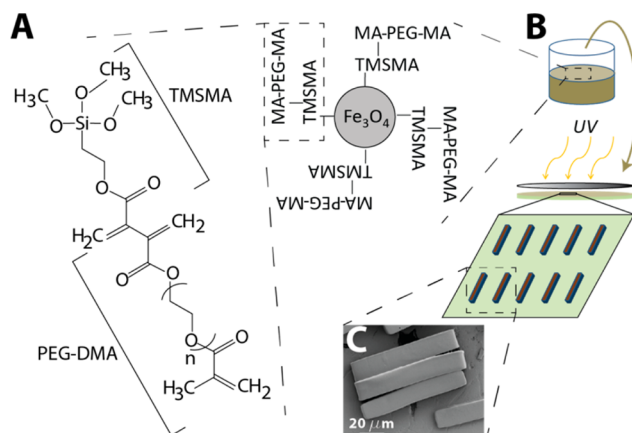
Figure 1. (A) In-house manufacture of the diblock copolymer poly(TMSMA-r-PEGDMA) facilitated coordination with iron-oxide nanoparticles during synthesis to coat and stabilize the magnetic nanoparticles. (B) Addition of coated nanoparticles to a solution of PEG–DMA with a cross-linking agent was used to generate magnetically active microstructures. (C) SEM of microstructures after harvesting from the silicon substrate.

in-house using an total iron assay kit (Biovision, Inc.) by the manufacturer's protocols.

Iron Oxide-Functionalized Magnetic Microrod Fabrication. Microrods were fabricated photolithographically by commercially available materials using methods adapted from previously designed protocols by our group and others, and are shown schematically in Figure 1B.[13,22,23,30] Silane-coated iron oxide nanoparticles were fabricated as described above and added in a 1:1 volume ratio to PEG–DMA (M_N 750, Sigma-Aldrich) and vortexed thoroughly. Microstructures were then created using standard photolithographic techniques (see the Supporting Information). Representative microrods are shown in the SEM in Figure 1C.

MRI Hardware. All MRI experiments were performed on a 7 T (310 mm bore size) superconducting magnet equipped with actively shielded imaging gradients (400 mT/m maximum gradient strength, 120 mm inner bore size) (Agilent Technologies, Palo Alto, CA).

^{1}H MRI of Magnetic Microrods. A. Vial Experiments. For ^{1}H imaging experiments, a 72 mm inner diameter quadrature ^{1}H birdcage resonator (Rapid Biomedical GmbH, Rimpar, Germany) was used for radio frequency pulse transmission and signal reception. Four vials were prepared with 0, 1×10^4, 2.5×10^4, and 1×10^5 iron-loaded microrods in water, centrifuged to the bottom, placed in a larger water filled container (size = 60 mm × 100 mm), and centered in the resonator. The water filled container was used to reduce the susceptibility differences around the microstructure containing vials. After localizer sequences, global shimming was performed with a 3D field-mapping sequence provided by the manufacturer's VnmrJ 3.1 scanner software (Agilent Technologies, Palo Alto, CA). To image the effect of the iron oxide nanoparticles on the MRI signal, a T1-weighted 2D multislice gradient echo sequence with different echo times was used: repetition time (TR) = 250 ms, echo times (TEs) = 2.7, 5.0, 15.0 ms, flip angle (α) = 30°, field of view (FOV) = 80 × 80 mm^2, matrix = 512 × 512, resolution = 156 × 156 μm^2, number of slices = 10, slice thickness = 1 mm, receiver bandwidth (BW) = 40.3 kHz, number of averages (NA) = 1.

B. In Vitro Chicken Heart Experiments. Commercially obtained chicken hearts were used as a model of solid tissue and injected with 50 μL aliquots of saline solution through a 30 gauge syringe carrying 1 × 10^5 iron-free microrods, 1 × 10^5 low-iron density microrods, or 1 × 10^5 high-iron density microrods. The hearts were then inserted into a conical plastic tube (diameter = 15 mm) and imaged with a custom-built 20 mm inner diameter linear ^{1}H birdcage resonator. After localizer sequences and global shimming, T1-weighted 2D multislice gradient echo images were acquired with the following parameters: TR = 250 ms, TE = 5 ms, α = 30°, FOV = 40 × 40 mm^2, matrix = 256 ×

256, resolution = 156 × 156 μm^2, number of slices = 12, slice thickness = 1 mm, BW = 40.3 kHz, NA = 1.

3D Manipulation of Magnetic Microrods. To study our ability to externally manipulate and align magnetic microrods in 3D environments, a rig was constructed to hold in place two juxtaposed 0.25 T neodymium magnets (3 in. diameter, 1.5 in. thick) with opposite poles facing one another at a small separation distance of less than 2 in. This creates a strong, unidirectional, and uniform permanent magnetic field between the two facing plates of the magnets. Magnetic microrods were then added to a liquid-phase solution of Matrigel (BD Biosciences) at ~4 °C. Matrigel is a thermally setting, ECM composite material that assumes tunable, tissue-relevant mechanical stiffnesses that are protein concentration dependent.[31] The Matrigel-microrod solution was then pipetted into an 8-well chamber-slide and placed in an incubator at 37 °C to gel. After 1 h, the slide was placed between the two large magnets at 37 °C and subsequently visualized under a microscope at 4, 12, and 24 h. Control cultures were plated under identical conditions but were never brought into contact with the magnetic field. Alignment was assessed through serial imaging of the entire depth of the gel and measuring angles of the long axis of the rod with respect to a defined reference line using ImageJ. This was done for n = 8 gels for each condition.

Fluorine-Tagged Microrod Fabrication. Fluorine-tagged microrods were made by methods similar to those described above, but with the incorporation of an acrylated, linear chain perfluorocarbon: 1H,1H,2H,2H-perfluorodecyl acrylate (PFA, Sigma). As detailed previously, PEG−DMA was mixed with the PFA at various inclusion volume ratios with cross-linking agent added, as above. The solution was vortexed and agitated thoroughly and continuously to maintain emulsification of the extremely hydrophobic PFA in solution. The solution was then immediately placed on a silicon wafer and underwent spin-coating and photolithography for 90 s at 8 mW/cm². Successful integration of fluorine into the microrod matrix was assessed by visual hydrophobicity of the microrods on the wafer. Fluorinated microrods were harvested as described previously and counted in preparation for MRI studies.

^{19}F MRI Experiments. *A. ^{19}F PFA Dilution Experiments.* ^{19}F spectroscopy and spectroscopic imaging was performed using a 2 cm diameter surface (loop) coil (Agilent Technologies, Palo Alto, CA) tunable between the ^{1}H frequency (300 MHz) and the ^{19}F (282 MHz) at 7 T. A ^{19}F NMR (nuclear magnetic resonance) spectrum from the polymerizable perfluorocarbon substance (raw) added to Eppendorf tubes and centered in the center of the surface coil was recorded using a pulse and acquire NMR sequence: TR = 10 s, BW = 100 kHz, number of complex points (NP) = 8192, NA = 8.

Detection sensitivity to PFA was determined by diluting into two lower concentrations using pure acetonitrile: (I) 0.47% (v/v% = 3.71 × 10^{-6} M or 6.31 × 10^{-5} N fluorine) and (II) 0.047% normal (3.71 × 10^{-7} M or 6.31 × 10^{-6} N fluorine). A classical chemical shift imaging (CSI) sequence, consisting of a hard-pulse (pulse length = 20 μs) followed by 3D phase-encoding and free-induction decay signal acquisition was used to localize and image the ^{19}F signal. Further parameters of the ^{19}F 3D CSI sequence: TR = 200 ms, TE = 160 μs, FOV = 32 × 32 × 32 mm³, matrix = 20 × 20 × 20, BW = 100 kHz, NP = 2048, NA = 1. The raw data of the ^{19}F CSI acquisition were processed with in-house written software programmed in Matlab (Matlab 2007a, Mathworks, Natick, MA). The raw data were filtered in the spatial domain using a hamming-window and in the spectral domain using a matched exponential-filter. Before 4D-Fourier transformation, data were zero-filled to 64 × 64 × 64 points in the spatial domain. To reconstruct images from the data sets, the spectral region between −1.36 and 2.20 kHz was integrated.

B. Localization of Perfluorocarbon-Loaded Microrods by ^{19}F MRI. Microrods were fabricated with a 0.47 v/v% of PFA in PEG−DMA to achieve strong detection capabilities. As with iron-loaded microrods, 1 × 10^5 PFA-labeled microrods were collected in a vial, and ^{19}F 3D CSI experiments were performed using the same protocols as above. Following the ^{19}F experiments, the surface coil was tuned to the ^{1}H frequency (without moving the vial in the MRI magnet), and ^{1}H MRI gradient echo reference images were acquired to verify the position of

the microrod collection in the vial. To assess sensitivity to detect a dispersed injection-type delivery of PFA-labeled microrods, 1 × 10^5 microrods were injected through a 30-gauge syringe needle into a vial filled with a solidified gelatin mold to emulate the mechanical qualities of soft tissue. Commercially obtained gelatin powder (3 oz.) was dissolved in 1 L of water by boiling, then dispensed into the vials and kept at 4 °C overnight to allow solidification. To facilitate visual confirmation of successful injection, red food coloring was added to the carrier fluid of the microstructure solution.

■ RESULTS

Localization of Iron-Loaded Microrods by ^{1}H MRI. The intensity of the signal cancelation generated by iron-labeled microstructures on a ^{1}H MR gradient echo sequence was observed to depend on the total iron content per voxel, which can be tuned either by adjusting the amount of iron incorporated into each microrod or by increasing the number of microrods injected into the target volume. Furthermore, the signal cancelation also depended on TE of the gradient echo MRI sequence and increased with increasing TEs. Up to an average of 3 pg of total iron was able to be incorporated per microrod without prohibitively interfering with the polymerization process (data not shown). Using these maximally iron-included microrods, we set out to test the minimum number of microrods that could be reliably detected by MRI.

Vial Experiments. The MRI signal cancelation due to the ferromagnetic iron was enhanced by increasing the TE from 2.7 to 15 ms. Figure 2 shows that the medium (M) and high (H)
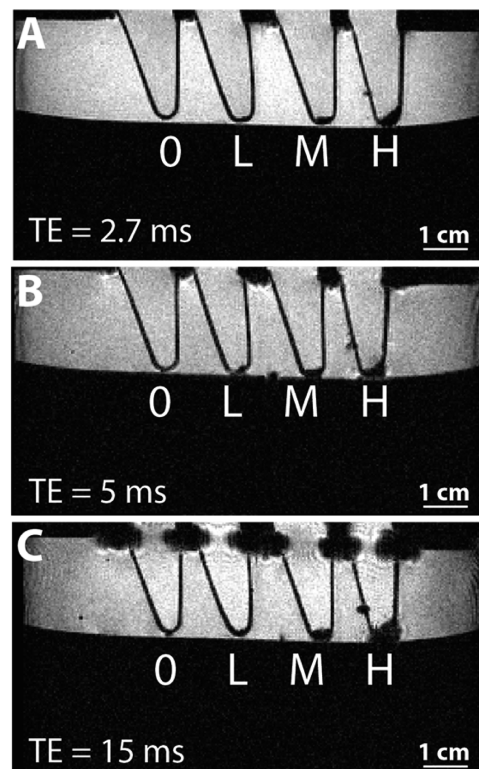
Figure 2. Microstructures functionalized with iron oxide nanoparticles are added to tubes in varying amounts of zero (0), 1 × 10^4 (L), 2.5 × 10^4 (M), and 1 × 10^5 (H). Images obtained using a gradient echo MRI sequence with echo times (TEs) of 2.7, 5, and 15 ms (A, B, and C, respectively) show increasing signal cancelation with increasing TE caused by the iron oxide embedded in the microstructures on the bottom of the tubes.

concentrations of microrods cause a visible MRI signal cancelation in images of all TEs. This signal dephasing effect increases at longer TEs. While the vial containing 1×10^4 microrods (L) shows only a small effect on the MRI signal at all TEs, no signal interference was visualized in the negative control vial (0). All four vials show a similar increased signal loss at the top with increasing TE where the vials contact the water in the container. The increased suscepibilty differences between water, air, and the plastic vial in this regions lead to this effect, especially at TE = 15 ms.

In Vitro Chicken Heart Experiments. We used commercially obtained chicken hearts as a model solid tissue in a custom designed coil (Supporting Information Figure S1). The chicken hearts carrying 1×10^5 iron-free microrods showed no decreased signal within the heart on the gradient echo MR images (Figure 3A). A small amount of air introduced at the entry of the injection tract led to a signal cancelation on the surface of the chicken heart (red arrow, Figure 3A). Low density iron-loaded microrod injections were clearly visualized in the heart tissue as shown in Figure 3B with the direction of injection indicated by the arrow. Two discrete, high density iron-loaded microrod injections are clearly seen in Figure 3C, demonstrating the spatial resolution of this imaging technique. The large, central regions of negative contrast in each image are caused by the air in the empty ventricular cavity of each heart.

3D Alignment of Iron-Loaded Microrods. Magnetically active microrods mixed in liquid-phase Matrigel assume a random orientation across the area and depth of the gel environment, as shown in Figure 4A (gel depth = 2 mm). By inserting the microrod-containing gel into a permanent magnetic field, alignment of the high-aspect ratio microrods with the magnetic field without translocation toward the magnets was achieved, due to the rotational torque imparted on the structure by the induced paramagnetic dipole (Figure 4C). The extent of microrod alignment was assessed by measurement of the angle of each rod in the field of view with respect to a consistently defined reference line and was shown to be random for iron-loaded microstructures in the absence of magnetic field as shown in the polar histogram in Figure 4B. Placing the gels in a permanent magnetic field for 15 h, however, resulted in very narrow alignment distributions almost completely concordant with the magnetic field direction (Figure 4D). Adding the control gels to the magnet or changing the orientation of the gels in the magnet resulted in realignment of the iron-loaded microstructures in the magnetic field within 4 h, demonstrating the dynamic potential of this method (Figure 4E).

^{19}F MRI. ^{19}F PFA Dilution Experiments. The ^{19}F NMR spectrum of the pure PFA (Supporting Information Figure S2) (polymerizable perfluorocarbon, 100% PFA = 3.16 M or 53.71 N with respect to fluorine) substance can be seen in Figure 5A. The highest resonance of the spectrum was chosen as reference and calibrated to 0 kHz on the frequency axis. The spectrum shows three more resonances upfield of the 0 kHz reference (at −0.31, −0.56, and −1.36 kHz) as well as two more resonances downfield (at 2.20 and 11.30 kHz). The results of the ^{19}F 3D CSI experiments to image the diluted PFA are shown in Figure 5. Figure 5B shows a color coded sagittal slice of the 3D data set of the 0.47% (v/v% = 3.71×10^{-6} M or 6.31×10^{-5} N fluorine) PFA solution. The signal was integrated over the spectral range between −1.36 and 2.20 kHz. Figure 5C shows the corresponding ^{19}F spectrum from one voxel in the high intensity signal area (red area) in Figure 5B. A sagittal image
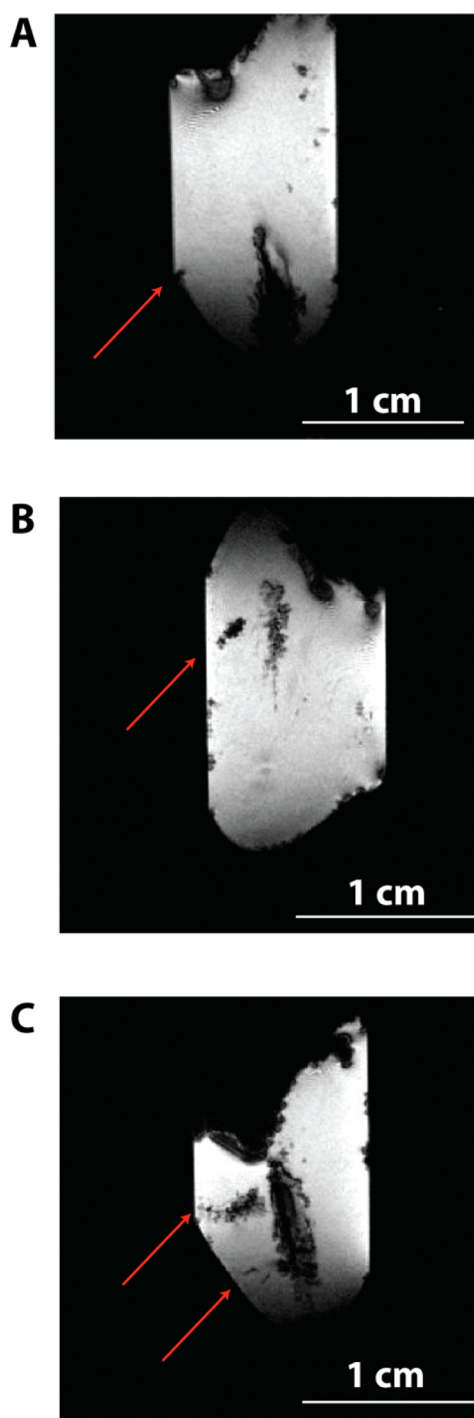
Figure 3. A custom built 20 mm diameter ^{1}H linear birdcage coil was used to image the chicken hearts injected with regular and magnetic microstructures. Sagittal view ^{1}H MRI gradient echo images (TR = 250 ms, TE = 5 ms) show no signal proximal to the injection site (red arrow) of nonfunctionalized microstructures (A). The injection of 1×10^4 microstructures carrying 0.6 pg of iron oxide each, however, yielded a small and defined area of signal cancelation in the images (B), while two injections of 1×10^4 magnetic microstructures carrying 2.7 pg of iron oxide each yielded areas of significant intramuscular signal decrease (C).

and the corresponding ^{19}F spectrum of a voxel of the 0.047% diluted solution (3.71×10^{-7} M or 6.31×10^{-6} N fluorine) can be seen in Figure 5D,E. In this spectrum, noise is visible on the
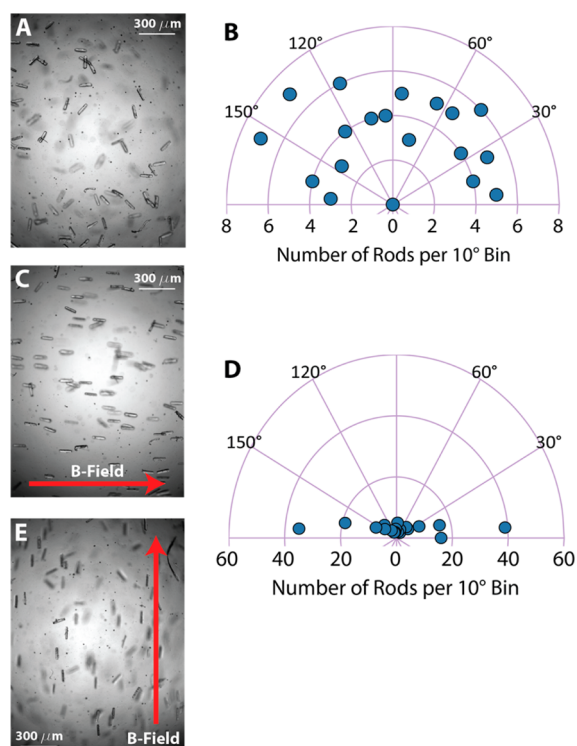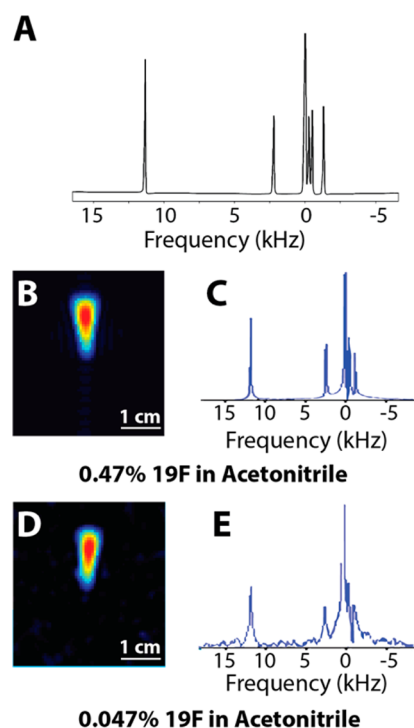
Figure 4. (A) Magnetic microstructures suspended in a 3D gel show random alignment with respect to each other, as quantified against a defined reference line in the polar plot (B). Microstructures in multiple image planes and gels were measured against the reference line along their long axis and binned into 10° increments, with the total number per group shown here. (C) Fifteen hours in a strong permanent magnetic field resulted in significant microstructure alignment in all planes, as quantified in (D). (E) Turning the gel 90° in the magnet resulted in realignment of the microstructures suspended in the gel after 4 h.


Figure 5. ^{19}F NMR spectrum of PFA substance is shown in (A). Results of the CSI experiments to localize diluted PFA in acetonitrile showed that the 0.47% v/v PFA solution yielded a strong ^{19}F signal. A sagittal ^{19}F image of the 3D data sets is shown in (B). This color coded image was reconstructed by integrating the spectral area between −1.36 and 2.20 kHz. The ^{19}F spectrum of one voxel is shown in (C). CSI experiments performed with a lower concentration of PFA in acetonitrile (0.047% v/v) reveal a decreased signal-to-noise ratio of the localized ^{19}F NMR spectrum, but still sufficient signal to localize and image the solution (D,E).

baseline, but the signal-to-noise ratios of the ^{19}F resonances are still excellent to localize and image the diluted PFA substance.

Localization of Perfluorocarbon-Loaded Microrods by ^{19}F MRI. Figure 6A shows the microrods fabricated with a 0.47 v/v % of PFA in PEG−DMA. The ^{1}H MR reference image in Figure 6B was acquired to verify the position of the microrod collection in the vial, which coincides with the concentrated signal detected by ^{19}F MRI, as shown in Figure 6C. A localized ^{19}F spectrum for the ^{19}F 3D CSI data set can be seen in Figure 6D. The spectrum shows the typical ^{19}F resonances from PCA, although the signal-to-noise ratio is decreased and the line widths of the resonances are broadened as compared to those of the raw substance.

The results of the injection of 1×10^5 PFA-labeled microrods into solidified gelatin mold are also shown in Figure 6. Figure 6E shows the successful injection of the microstructure solution colored by red food coloring into the gelatin mold to aid visualization. The ^{1}H MR reference image showed no signal enhancement of the region injected with the hydrogel polymer microstructures (Figure 6F), whereas ^{19}F 3D CSI showed a distribution consistent with that seen visually after injection (Figure 6G). Figure 6H shows an overlay of the color coded ^{19}F image on the gray scale ^{1}H image. Figure 6I shows the localized ^{19}F NMR spectrum from the CSI data set. The ^{19}F PFA resonances are visible as a sensitive and specific region of

positive contrast, albeit with a decreased signal-to-noise ratio as compared to that of the raw substance.

■ DISCUSSION

The increasing use of "smart materials" and advanced functionalized polymer technologies for therapeutic applications has necessitated the incorporation of a wide variety of mechanical, chemical, and biological qualities into existing materials to adapt them for the numerous and unique challenges of the physiologic environment.[2,3,6,9,15,17,32] As the application of polymer biomaterials to the growing field of smart material technologies moves away from stand-alone surface coatings or delivery vehicles and begins to become more functional, tissue-integrated therapeutic platforms, challenges in safety and noninvasive implementation and monitoring of these material strategies will become vital. Here, we propose two such functionalizations that serve to (1) introduce capabilities of remote manipulation for improved in vitro study and in vivo integration of discrete polymeric microstructural materials, and (2) provide a means by which to track and image microscale polymer therapeutics.

High aspect microstructures, such as microrods, have been shown to have the potential to instruct cell orientation and tissue growth in 2D applications.[15,32−34] One limitation of introducing any type of polymeric tissue engineering platform that promotes cellular integration or tissue regeneration is the prospect of disorganized growth. In the heart, for example, the
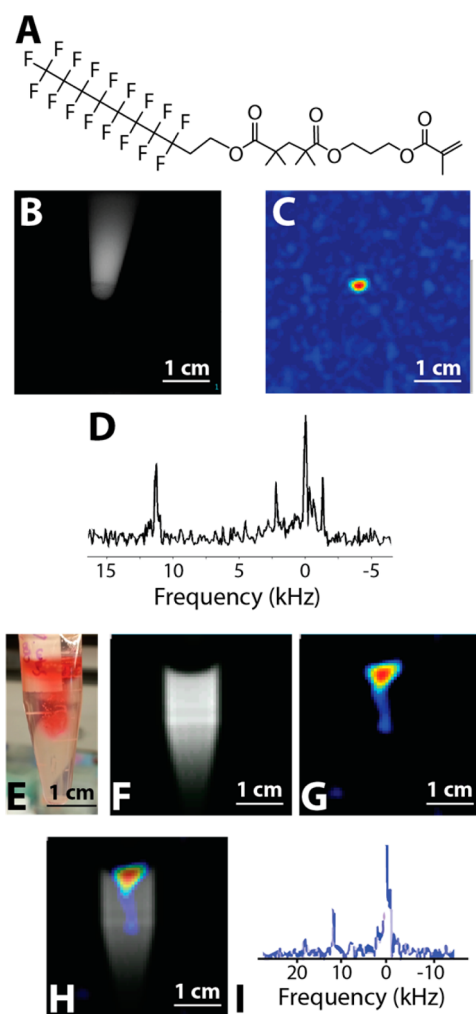
Figure 6. PEG–DMA was chemically functionalized with PFA to generate a fluorinated polymer molecule (A). As previously, 100 000 microstructures photo-cross-linked in the presence of PFA–PEG–DMA and collected at the bottom of a centrifuge tube to be imaged by ^{1}H MRI (B) and ^{19}F MRI (3D CSI) (C), yielding localized ^{19}F NMR spectra that show the typical, but broadened PFA resonances as compared to the raw substance (D). A gelatin mold was formed in a tube and injected with 100 000 fluorinated microstructures in the presence of nonfluorine-containing red dye (E). The ^{1}H MR reference image showed no signal changes after the injection (F), while ^{19}F 3D CSI located the microrod collection in an identical distribution as seen visually (G) and shown in the ^{19}F overlay image on the ^{1}H image (H). The localized ^{19}F NMR spectrum in the injected area confirmed the signal source as the incorporated PFA molecules (I).

orientation of cell–cell contacts to create linear tissue planes for electrical conduction is vital to the physiologic function of the heart, as disorganized tissue growth can serve as a nidus for electrical anomalies. Here, we demonstrate that iron-functionalized microrods can be externally manipulated by magnetic fields in 3D to create aligned polymeric scaffolds that can be integrated into any tissue environment. The magnetic functionalization of discrete polymeric microstructures adds a new dimension to the potential utility of these materials in the setting of in vitro tissue engineering and as a means to provide physical cues for in vivo regenerative applications. Adding magnetic functionalization to discrete polymeric cues makes it possible to create organized scaffolds across a 3D volume. This capability will facilitate study into how cells organize and

respond to microstructural cues in a physiologic extracellular matrix and will pave the way for better understanding of how to engineer organized tissues for regenerative strategies.

In addition to its use in settings of remote microstructure alignment for instructional tissue engineering cues, MRI technologies provide a parallel functionality for these magnetized polymeric devices. Iron-based nanoparticles have long been used as a contrast agent for MRI applications, including cell labeling or vascular enhancement.[21,35−40] Iron oxide nanoparticles are easy to produce at low cost and have the added advantage of being relatively benign to tissue when delivered in small amounts,[41] thanks in part to the significant iron carrying capacity of the blood. This has been further supported by the fact that we see no changes in cell metabolism or cell death when cultured in contact with large quantities of our iron-loaded microstructures for a variety of cell types (Supporting Information Figure S3). When incorporated into the polymer matrix, iron-oxide nanoparticles make it possible to locate and track polymeric devices in situ by MRI, giving insight into the safety profile, longevity, and targeting accuracy of this noninvasively delivered therapeutic. The ability to track these microstructures was also confirmed in a mock injection into substitute tissue, as physiologic injections of discrete polymeric microstructures may not be confined to a concentrated area depending on the density of the target tissue and the volume of the fluid injection delivered. The results shown with this work suggest that this system can, indeed, reliably track dispersed iron-loaded microstructures and has potential utility in the setting of a tissue-based injection.

The adaptation of previously developed polymer coating methods for iron oxide nanoparticles facilitates their stable incorporation into polymer microstructures, which is critical to their utility in tissue engineering applications. The covalent, methacrylate-based chemical bonds of PEG–DMA are extremely strong in physiologic environments, and there is evidence that they can last for several years before being hydrolyzed.[3,26] This, in turn, means that the iron oxide nanoparticles can be affixed to the polymer matrix and remain bound to the microstructures for the lifetime of the material device, enabling long-term tracking and even calibrated determination of degradation rates of the functionalized polymer material. Other groups have shown similar iron oxide nanoparticulate composite polymers, but, as many of these are designed for hyperthermic drug delivery and often involve bulk polymerization or more rapidly hydrolyzed materials, the potential lifetime of an iron-included polymeric microdevice utilizing covalent incorporation remains unclear.[42−44] Furthermore, due to the discretized nature of our low concentration microstructured composites and the use of slow-acting permanent magnetic fields, we have not seen evidence of environmental damage or heating due to the motion of the microrods. This includes no observed temperature change in a Matrigel culture loaded with magnetic microrods and exposed to a high frequency oscillating electromagnetic field (data not shown) and no evidence of microstructure translocation or structural damage to a gel scaffold in the presence of strong magnetic fields over long incubation periods of 4−15 h (Figure 4). However, further investigation would be valuable to evaluate the precise kinetics of the release of the iron oxide nanoparticles from the bound polymer matrix and the magnetic threshold for effective translocation or rapid movement of the microstructures that could potentially precipitate tissue damage. We continue to

evaluate these characteristics to better understand the role these factors play in device longevity and potential toxicity.

It is important to consider, however, that iron incorporation serves as a negative contrast (signal cancelation) agent for MRI applications as it shortens the transversal relaxation times of the local protons due to the induced dipole in the iron oxide matrix. This interference is not specific and can be difficult to differentiate from other sources, which decrease the transversal relaxation times, such as clotted blood or air, as is illustrated in Figure 3A−C. This may limit the scope of applicability of this type of contrast agent, depending on the characteristics of the therapeutic target tissue, and requires a careful investigation of the signal decay source with respect to the chosen TE for the experiments. Besides intrinsic origins (like blood or air), which affect the transversal relaxation time, apparatus-specific sources (insufficient field homogeneity) can also lead to signal decay in the MR gradient echo images. Furthermore, it may not always be possible to filter out these sources of signal cancelation, obscuring the view of surrounding tissues that may hinder the diagnostic reliability contrast generation based on iron-oxide particles in combination with ^{1}H MRI.

The use of a specific and sensitive positive contrast agent, such as ^{19}F molecules, presents an elegant solution to the challenges of iron-oxide contrast agents, which provide signal cancelation as a contrast mechanism. The ^{19}F nucleus has a NMR sensitivity of 83% relative to the ^{1}H and is therefore one of the most sensitive nuclei for NMR. Because the amount of physiologic ^{19}F-containing compounds in biological tissue is negligible, ^{19}F NMR and MRI are not hampered by interference from background signals.[45−48] Long-chain fluorocarbons can be attached to an array of chemical functional groups, making this strategy viable for polymers beyond the PEG−DMA polymer described here. However, considerations of decreased mobility of the long-chain fluorine molecule once it is polymerized into the PEG−DMA matrix, thus experiencing a more physically constrained environment leading to spectral peak broadening (and therefore shortened transversal relaxation time), are necessary to utilize this method effectively. Considerable research has been pursued in developing fluorinated nano-particulate emulsions for tracking or targeting cancers and inflammation, but these approaches encounter additional challenges in targeting, longevity, and toxicity.[49−51] By stably and covalently tagging injectable microstructured polymer materials with small amounts of these compounds as shown in this work, the therapeutic devices could be reliably located and monitored over time to ensure proper implantation and positioning of the device throughout its lifetime with limited exposure and distribution to other nontargeted tissues.

The chemical nature of long-chain fluorocarbons, however, does potentially present challenges to therapeutic implementation. The toxicity of some fluorinated molecules has been studied, and many PFCs are considered biologically inert, but specific examination of the molecules used for targeting is necessary.[52−54] Although our method covalently bonds the molecules to the polymer matrix of the device, most injectable polymer devices are not designed to be explanted as the degradation products are generally biocompatible and effective collection of the material that is integrated into the tissue is not possible. In this case, any conjugated fluorinated molecules, even in the extremely small quantities described here, would need to be similarly nonreactive and nonprovoking of an immune response upon degradation. However, it is likely that the long-term degradation profile of polymers such as PEG−

DMA would result in extremely small amounts of fluorinated polymer released at any given time and would remain at subtoxic levels and be cleared safely by the body.

We have examined the response of fibroblasts to our fluorinated microrods in vitro, showing little effect on cell metabolism in the presence of a large number of low-fluorine concentration microrods (sufficient levels for imaging, as seen in Figure 6), but higher levels of fluorine do adversely affect cell growth, either by toxic chemical effects or by alterations in surface binding due to the hydrophobic nature of the molecule (Supporting Information Figure S3). Further examination of the biological effects and appropriate doses of this material will be important for its eventual implantation in vivo.

■ CONCLUSION

We have developed two strategies for chemical functionalization of polymeric microstructures to enable remote manipulation of discrete devices and sensitive detection of implanted polymer materials by MRI methods. Polymer hydrogel materials possess a broad range of therapeutic potentials, and the ability to incorporate advanced mechanical and chemical integrations is vital to their continued pioneering into new tissue engineering applications. The inclusion of iron oxide paves the way for remote manipulation of polymer materials in three dimensions with a precision that is unachievable with traditional polymer materials, introducing the ability to generate organized constructs in 3D tissue space. Simultaneously, this functionalization allows sensitive MRI detection of materials, even when dispersed across large regions of tissue after injection, which can facilitate safe, long-term in vivo monitoring of polymeric devices that were previously invisible after implantation. Additional functionalization with PFCs, meanwhile, utilizes exciting new applications of MRI technologies to provide extremely sensitive and specific labeling of polymeric devices to enable clinical monitoring of even micrometer-scale implanted polymer devices. Functionalizations such as these can be applied across a broad spectrum of polymer solutions for tissue engineering and materials-based therapies and will continue to tap into the near limitless mechanical, chemical, and biological potentials of engineered polymers for translational applications.

■ ASSOCIATED CONTENT

ⓢ Supporting Information

Additional details on methods, accessory data on in vitro biocompatibility profile, and continued discussion. This material is available free of charge via the Internet at http://pubs.acs.org.

■ AUTHOR INFORMATION

Corresponding Author

*E-mail: tejal.desai@ucsf.edu.

Notes

The authors declare no competing financial interest.

■ ACKNOWLEDGMENTS

■ ABBREVIATIONS

MRI, magnetic resonance imaging; NMR, nuclear magnetic resonance; PEG−DMA, polyethylene glycol dimethacrylate; PFA, $1H,1H,2H,2H$-perfluorodecyl acrylate; PFCs, perfluorocarbons; SEM, scanning electron microscope; TMSMA, 3-(trimethoxysilylpropyl methacrylate); poly(TMSMA-r-PEGD-MA), diblock copolymer of TMSMA and PEG−DMA; ^1H MRI, proton magnetic resonance imaging; ^{19}F MRI, fluorine magnetic resonance imaging; 3D, three-dimensional

■ REFERENCES

(1) Chen, H.; Yuan, L.; Song, W.; Wu, Z.; Li, D. Biocompatible Polymer Materials: Role of Protein−surface Interactions. *Prog. Polym. Sci.* **2008**, *33*, 1059−1087.

(2) Jagur-grodzinski, J. Polymers for Tissue Engineering, Medical Devices, and Regenerative Medicine. Concise General Review of Recent Studies. *Polym. Adv. Technol.* **2006**, *17*, 395−418.

(3) Ulery, B. D.; Nair, L. S.; Laurencin, C. T. Biomedical Applications of Biodegradable Polymers. *J. Polym. Sci., Part B: Polym. Phys.* **2011**, *49*, 832−864.

(4) Baszkin, A.; Lyman, D. J. The Interaction of Plasma Proteins with Polymers - Relationship Between Polymer Surface Energy and Protein Adsorption/desorption. *J. Biomed. Mater. Res.* **1980**, *14*, 393−403.

(5) Tao, S. L.; Desai, T. A. Microfabricated Drug Delivery Systems: From Particles to Pores. *Adv. Drug Delivery Rev.* **2003**, *55*, 315−328.

(6) Qiu, Y.; Park, K. Environment-Sensitive Hydrogels for Drug Delivery. *Adv. Drug Delivery Rev.* **2001**, *53*, 321−339.

(7) Hoare, T. R.; Kohane, D. S. Hydrogels in Drug Delivery: Progress and Challenges. *Polymer* **2008**, *49*, 1993−2007.

(8) Doraiswamy, A.; Jin, C.; Narayan, R. J.; Mageswaran, P.; Mente, P.; Modi, R.; Auyeung, R.; Chrisey, D. B.; Ovsianikov, A.; Chichkov, B. Two Photon Induced Polymerization of Organic-Inorganic Hybrid Biomaterials for Microstructured Medical Devices. *Acta Biomater.* **2006**, *2*, 267−275.

(9) Middleton, J. C.; Tipton, A. J. Synthetic Biodegradable Polymers as Orthopedic Devices. *Biomaterials* **2000**, *21*, 2335−2346.

(10) Tee, R.; Lokmic, Z.; Morrison, W. A.; Dilley, R. J. Strategies in Cardiac Tissue Engineering. *Aust. N. Z. J. Surg.* **2010**, *80*, 683−693.

(11) Boateng, S. Y.; Hartman, T. J.; Ahluwalia, N.; Vidula, H.; Desai, T. A.; Russell, B. Inhibition of Fibroblast Proliferation in Cardiac Myocyte Cultures by Surface Microtopography. *Am. J. Physiol.: Cell Physiol.* **2003**, *285*, C171−82.

(12) Cong, H.; Revzin, A.; Pan, T. Non-Adhesive PEG Hydrogel Nanostructures for Self-Assembly of Highly Ordered Colloids. *Nanotechnology* **2009**, *20*, 075307.

(13) Curtis, M.; Sharma, S.; Desai, T.; Russell, B. Hypertrophy, Gene Expression, and Beating of Neonatal Cardiac Myocytes Are Affected by Microdomain Heterogeneity in 3D. *Biomed. Microdevices* **2010**, *12*, 1073−1085.

(14) Engelmayr, G. C.; Papworth, G. D.; Watkins, S. C.; Mayer, J. E.; Sacks, M. S. Guidance of Engineered Tissue Collagen Orientation by Large-Scale Scaffold Microstructures. *J. Biomech.* **2006**, *39*, 1819−1831.

(15) Norman, J. J.; Desai, T. A. Methods for Fabrication of Nanoscale Topography for Tissue Engineering Scaffolds. *Ann. Biomed. Eng.* **2006**, *34*, 89−101.

(16) Christman, K. L.; Vardanian, A. J.; Fang, Q.; Sievers, R. E.; Fok, H. H.; Lee, R. J. Injectable Fibrin Scaffold Improves Cell Transplant Survival, Reduces Infarct Expansion, and Induces Neovasculature Formation in Ischemic Myocardium. *J. Am. Coll. Cardiol.* **2004**, *44*, 654−660.

(17) Plotkin, M.; Vaibavi, S. R.; Rufaihah, A. J.; Nithya, V.; Wang, J.; Shachaf, Y.; Kofidis, T.; Seliktar, D. The Effect of Matrix Stiffness of Injectable Hydrogels on the Preservation of Cardiac Function after a Heart Attack. *Biomaterials* **2014**, *35*, 1429−1438.

(18) Purcell, B. P.; Lobb, D.; Charati, M. B.; Dorsey, S. M.; Wade, R. J.; Zellars, K. N.; Doviak, H.; Pettaway, S.; Logdon, C. B.; Shuman, J. A.; et al. Injectable and Bioresponsive Hydrogels for on-Demand Matrix Metalloproteinase Inhibition. *Nat. Mater.* **2014**, *13*, 653−661.

(19) Rane, A. a; Chuang, J. S.; Shah, A.; Hu, D. P.; Dalton, N. D.; Gu, Y.; Peterson, K. L.; Omens, J. H.; Christman, K. L. Increased Infarct Wall Thickness by a Bio-Inert Material Is Insufficient to Prevent Negative Left Ventricular Remodeling after Myocardial Infarction. *PLoS One* **2011**, *6*, e21571.

(20) Seif-Naraghi, S. B.; Salvatore, M. A.; Schup-Magoffin, P. J.; Hu, D. P.; Christman, K. L. Design and Characterization of an Injectable Pericardial Matrix Gel: a Potentially Autologous Scaffold for Cardiac Tissue Engineering. *Tissue Eng., Part A* **2010**, *16*, 2017−2027.

(21) Amsalem, Y.; Mardor, Y.; Feinberg, M. S.; Landa, N.; Miller, L.; Daniels, D.; Ocherashvili, A.; Holbova, R.; Yosef, O.; Barbash, I. M.; et al. Iron-Oxide Labeling and Outcome of Transplanted Mesenchymal Stem Cells in the Infarcted Myocardium. *Circulation* **2007**, *116*, I38−45.

(22) Ayala, P.; Lopez, J.; Desai, T. Microtopographical Cues in 3D Attenuate Fibrotic Phenotype and Extracellular Matrix Deposition: Implications for Tissue Regeneration. *Tissue Eng., Part A* **2010**, *16*, 2519−2527.

(23) Collins, J. M.; Ayala, P.; Desai, T. A.; Russell, B. Three-Dimensional Culture with Stiff Microstructures Increases Proliferation and Slows Osteogenic Differentiation of Human Mesenchymal Stem Cells. *Small* **2010**, *6*, 355−360.

(24) Jawad, H.; Lyon, A. R.; Harding, S. E.; Ali, N. N.; Boccaccini, A. R. Myocardial Tissue Engineering. *Br. Med. Bull.* **2008**, *87*, 31−47.

(25) Meenach, S. A.; Anderson, K. W.; Hilt, J. Z. Synthesis and Characterization of Thermoresponsive Poly(Ethylene Glycol)-Based Hydrogels and Their Magnetic Nanocomposites. *Polymer* **2010**, *48*, 3229−3235.

(26) Lin-Gibson, S.; Bencherif, S.; Cooper, J. A.; Wetzel, S. J.; Antonucci, J. M.; Vogel, B. M.; Horkay, F.; Washburn, N. R. Synthesis and Characterization of PEG Dimethacrylates and Their Hydrogels. *Biomacromolecules* **2004**, *5*, 1280−1287.

(27) Lee, H.; Lee, E.; Kim, D. K.; Jang, N. K.; Jeong, Y. Y.; Jon, S. Antibiofouling Polymer-Coated Superparamagnetic Iron Oxide Nanoparticles as Potential Magnetic Resonance Contrast Agents for in Vivo Cancer Imaging. *J. Am. Chem. Soc.* **2006**, *128*, 7383−7389.

(28) Lee, H.-Y.; Lee, S.-H.; Xu, C.; Xie, J.; Lee, J.-H.; Wu, B.; Koh, A. L.; Wang, X.; Sinclair, R.; Wang, S. X.; et al. Synthesis and Characterization of PVP-Coated Large Core Iron Oxide Nanoparticles as an MRI Contrast Agent. *Nanotechnology* **2008**, *19*, 165101.

(29) Zhu, S.; Marschilok, A. C.; Takeuchi, E. S.; Yee, G. T.; Wang, G.; Takeuchi, K. J. Nanocrystalline Magnetite: Synthetic Crystallite Size Control and Resulting Magnetic and Electrochemical Properties. *J. Electrochem. Soc.* **2010**, *157*, A1158−1163.

(30) Kim, Y. S.; Suh, K. Y.; Lee, H. H. Fabrication of Three-Dimensional Microstructures by Soft Molding. *Appl. Phys. Lett.* **2001**, *79*, 2285.

(31) Kleinman, H. K.; Martin, G. R. Matrigel: Basement Membrane Matrix with Biological Activity. *Semin. Cancer Biol.* **2005**, *15*, 378−386.

(32) Kim, P.; Kim, D. H.; Kim, B.; Choi, S. K.; Lee, S. H.; Khademhosseini, A.; Langer, R.; Suh, K. Y. Fabrication of Nanostructures of Polyethylene Glycol for Applications to Protein Adsorption and Cell Adhesion. *Nanotechnology* **2005**, *16*, 2420−2426.

14484

dx.doi.org/10.1021/am503778t | *ACS Appl. Mater. Interfaces* 2014, 6, 14477−14485

(33) Suh, K. A Simple Soft Lithographic Route to Fabrication of Poly(ethylene Glycol) Microstructures for Protein and Cell Patterning. *Biomaterials* **2004**, *25*, 557–563.

(34) Motlagh, D.; Hartman, T. J.; Desai, T. A.; Russell, B. Microfabricated Grooves Recapitulate Neonatal Myocyte Connexin43 and N-Cadherin Expression and Localization. *J. Biomed. Mater. Res., Part A* **2003**, *67*, 148–157.

(35) Gupta, A. K.; Gupta, M. Synthesis and Surface Engineering of Iron Oxide Nanoparticles for Biomedical Applications. *Biomaterials* **2005**, *26*, 3995–4021.

(36) Krishnan, K. M. Advances in Magnetics Biomedical Nano-magnetics: A Spin Through Possibilities in Imaging, Diagnostics, and Therapy. *Magn. IEEE Trans.* **2010**, *46*, 2523–2558.

(37) Pankhurst, Q. A.; Connolly, J.; Jones, S. K.; Dobson, J. Applications of Magnetic Nanoparticles in Biomedicine. *J. Phys. D: Appl. Phys.* **2003**, *36*, R167–R181.

(38) Rad, A. M.; Arbab, A. S.; Iskander, A. S. M.; Jiang, Q.; Soltanian-Zadeh, H. Quantification of Superparamagnetic Iron Oxide (SPIO)-Labeled Cells Using MRI. *J. Magn. Reson. Imaging* **2007**, *26*, 366–374.

(39) Sun, C.; Lee, J. S. H.; Zhang, M. Magnetic Nanoparticles in MR Imaging and Drug Delivery. *Adv. Drug Delivery Rev.* **2008**, *60*, 1252–1265.

(40) Tromsdorf, U. I.; Bruns, O. T.; Salmen, S. C.; Beisiegel, U.; Weller, H. A Highly Effective, Nontoxic T1MR Contrast Agent Based on Ultrasmall PEGylated Iron Oxide Nanoparticles. *Nano Lett.* **2009**, *9*, 4434–4440.

(41) Mahmoudi, M.; Simchi, A.; Milani, A. S.; Stroeve, P. Cell Toxicity of Superparamagnetic Iron Oxide Nanoparticles. *J. Colloid Interface Sci.* **2009**, *336*, 510–518.

(42) Meenach, S. A.; Shapiro, J. M.; Hilt, J. Z.; Anderson, K. W. Characterization of PEG-Iron Oxide Hydrogel Nanocomposites for Dual Hyperthermia and Paclitaxel Delivery. *J. Biomater. Sci., Polym. Ed.* **2013**, *24*, 1112–1126.

(43) Bardajee, G. R.; Hooshyar, Z. One-Pot Synthesis of Biocompatible Superparamagnetic Iron Oxide Nanoparticles/hydrogel Based on Salep: Characterization and Drug Delivery. *Carbohydr. Polym.* **2014**, *101*, 741–751.

(44) Zhang, Y.; Sun, Y.; Yang, X.; Hilborn, J.; Heerschap, A.; Ossipov, D. Injectable In Situ Forming Hybrid Iron Oxide-Hyaluronic Acid Hydrogel for Magnetic Resonance Imaging and Drug Delivery. *Macromol. Biosci.* **2014**, Epub ahead of print.

(45) Bulte, J. W. M. Hot Spot MRI Emerges from the Background. *Nat. Biotechnol.* **2005**, *23*, 945–946.

(46) Ruiz-Cabello, J.; Barnett, B. P.; Bottomley, P. A.; Bulte, J. W. M. Fluorine (19F) MRS and MRI in Biomedicine. *NMR Biomed.* **2011**, *24*, 114–129.

(47) Díaz-López, R.; Tsapis, N.; Fattal, E. Liquid Perfluorocarbons as Contrast Agents for Ultrasonography and (19)F-MRI. *Pharm. Res.* **2010**, *27*, 1–16.

(48) Martino, R.; Gilard, V.; Desmoulin, F.; Malet-Martino, M. Fluorine-19 or Phosphorus-31 NMR Spectroscopy: a Suitable Analytical Technique for Quantitative in Vitro Metabolic Studies of Fluorinated or Phosphorylated Drugs. *J. Pharm. Biomed. Anal.* **2005**, *38*, 871–891.

(49) Bae, P. K.; Jung, J.; Lim, S. J.; Kim, D.; Kim, S. K.; Chung, B. H. Bimodal Perfluorocarbon Nanoemulsions for Nasopharyngeal Carcinoma Targeting. *Mol. Imaging Biol.* **2013**, *15*, 401–410.

(50) Srinivas, M.; Cruz, L. J.; Bonetto, F.; Heerschap, A.; Figdor, C. G.; de Vries, I. J. M. Customizable, Multi-Functional Fluorocarbon Nanoparticles for Quantitative in Vivo Imaging Using 19F MRI and Optical Imaging. *Biomaterials* **2010**, *31*, 7070–7077.

(51) Giraudeau, C.; Geffroy, F.; Meriaux, S.; Boumezbeur, F.; Robert, P.; Port, M.; Robic, C.; Le Bihan, D.; Lethimonnier, F.; Valette, J. 19F Molecular MR Imaging for Detection of Brain Tumor Angiogenesis: In Vivo Validation Using Targeted PFOB Nanoparticles. *Angiogenesis* **2013**, *16*, 171–179.

(52) Lutz, J.; Kettemann, M.; Rácz, I.; Nöth, U. Several Methods Utilized for the Assessment of Bio-Compatibility of Perfluorochemicals. *Artif. Cells, Blood Substitutes, Biotechnol.* **1995**, *23*, 407–415.

(53) Janjic, J. M.; Shao, P.; Zhang, S.; Yang, X.; Patel, S. K.; Bai, M. Perfluorocarbon Nanoemulsions with Fluorescent, Colloidal and Magnetic Properties. *Biomaterials* **2014**, *35*, 4958–4968.

(54) Peng, H.; Blakey, I.; Dargaville, B.; Rasoul, F.; Rose, S.; Whittaker, A. K. Synthesis and Evaluation of Partly Fluorinated Block Copolymers as MRI Imaging Agents. *Biomacromolecules* **2009**, *10*, 374–381.

14485

dx.doi.org/10.1021/am503778t | *ACS Appl. Mater. Interfaces* 2014, 6, 14477–14485